INFN-LNL-257(2019)

Progetto PASTA

Production with Accelerator of Scandium-47

for Theranostic Applications

Report 2018

OUTLINE

1. Progetto PASTA – 2018

FTE 2018

	LNL		FE		PD
Gaia Pupillo	1.0	Micòl Pasquali	0.8	Luciano Canton	0.1
Liliana Mou	0.5	Alessandra Boschi	0.5		**PV**
Petra Martini	0.5	Adriano Duatti	0.5	Andrea Fontana	0.2

Collaborazione esterna presso Arronax (Nantes, Francia): Ferid Haddad, Cyrille Alliot, Thomas Sounalet.

4.1 FTE totali.

FINANZIAMENTO E RENDICONTAZIONE DI SPESA

PASTA 2018	LNL (k€)
MISSIONI* Irraggiamenti ad Arronax (Nantes, Francia) + congresso Varenna	8 + 1.5 = 9.5
CONSUMO** Materiale arricchito (Ti-49 e Ti-50)	15 + 8 = 23
TRASPORTO*** Trasporto radioattivo da Arronax (Nantes) a LNL (PD, Italy)	3
ATTREZZATURE**** Redistribuzione fondi 2017	0.8
Totale Progetto PASTA 2018	**36.3**

* Un fondo aggiuntivo pari a 1.5 k€ è stato richiesto ed ottenuto per partecipazione su invito a congresso Varenna (Giugno 2018)

** A Gennaio 2018 è stato richiesto ed ottenuto un fondo aggiuntivo per l'acquisto di materiale arricchito pari a 8 k€; il progetto E_PLATE ha contribuito all'acquisto del materiale arricchito con ulteriori 4.3 k€; spesa totale acquisto Titanio arricchito (300 mg Ti-49 and 150 mg Ti-50 Oak Ridge National Laboratories): 27.3 k€

*** I fondi della voce TRASPORTO (3 k€) sono stati stornati su ATTREZZATURE del progetto Laramed

**** I fondi della voce ATTREZZATURE (0.8 k€) sono stati stornati su ATTREZZATURE del progetto Laramed

Lo storno su ATTREZZATURE del progetto Laramed, avvenuto previo consenso dei referees e del Presidente di CSN5, copre la spesa dell'acquisto delle giare in zirconia (costo circa 2.5 k€ + IVA) per la criomacinazione del titanio arricchito; il costo totale per l'acquisto del criomulino, incluse le giare in acciaio e zirconia, è pari circa 10.5 k€ + IVA (fondi Laramed ATTREZZATURE).

MILESTONE 2018

31-07-2018 – Conclusione turni di irraggiamento su target di Ti-48

- No. 6 run ad Arronax, per la misura delle reazioni nucleari $^{nat}V(p,x)^{47}Sc$ e $^{48}Ti(p,x)^{47}Sc$ (Table 1)

30-09-2018 – Test chimico di estrazione di sc-47 da bersaglio di Titanio irraggiato

- Procedura radiochimica di separazione Sc/Ti sviluppata a freddo; test ICP-OES (Table 7)

31-12-2018 - Conclusione turni di irraggiamento su target di Ti-50

I BERSAGLI DI TI-50 NON SONO STATI REALIZZATI ENTRO IL 2018 CAUSA MATERIALE ARRICCHITO ACQUISTATO IN FORMA DI SPUGNA METALLICA ANZICHÉ POLVERE METALLICA (**FIGURE 6–**

- Figure 11)

2. Scientific Activity (year 2018)

REALIZATION OF METALLIC TARGETS OF ENRICHED TITANIUM

ENRICHED Ti-48 METALLIC DEPOSIT

During 2017 the HIVIPP method (HIgh energy VIbrational Powder Plating) was used to realize the enriched target foils irradiated at the Arronax facility, by using the prototype HIVIPP machine developed at LNL to have a thin deposit of enriched ^{48}Ti metal powder (purchased by TraceScience) on Al support (25 µm thick). During 2018 the HIVIPP technique was optimized/better investigated by Hanna Skliarova through the E_PLATE (Electrostatic Powders pLating for Accelerator TargEts) project.

FIGURE 1. SCHEME OF THE HIVIPP DEPOSITION SYSTEM INSIDE THE VACUUM CHAMBER (LEFT) AND A PHOTOGRAPH OF THE DEPOSITION SYSTEM WITH AL SUBSTRATES AND ^{48}TI METALLIC POWDER INSIDE THE QUARTZ CYLINDER (RIGHT). COURTESY OF E_PLATE PROJECT (H. SKLIAROVA)

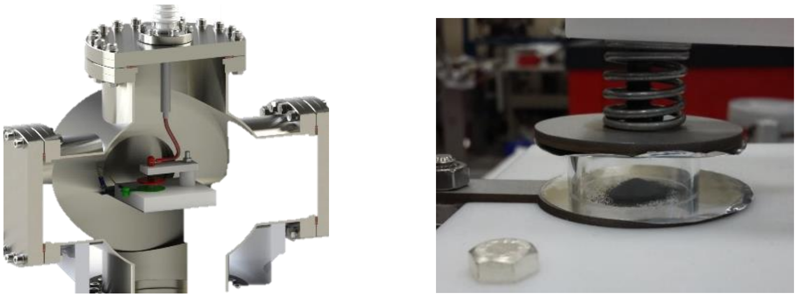

FIGURE 2. PHOTOGRAPH OF A TYPICAL TARGET PREPARATION OF ^{48}TI METALLIC POWDER DEPOSITED ON AL SUBSTRATE; NO DAMAGE IS VISIBLE AFTER THE IRRADIATION RUN AT THE ARRONAX FACILITY

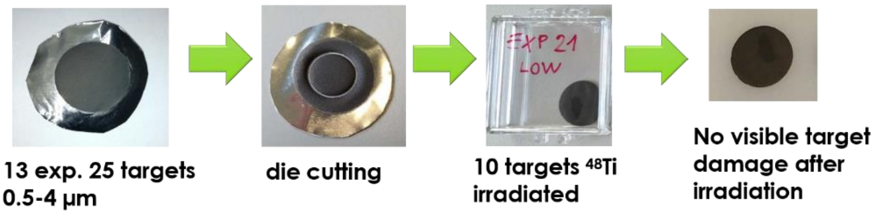

Figure 3. SEM powders and deposit analysis on 25 μm thick Al support of ^{NAT}Ti (left) and ^{48}Ti (right)

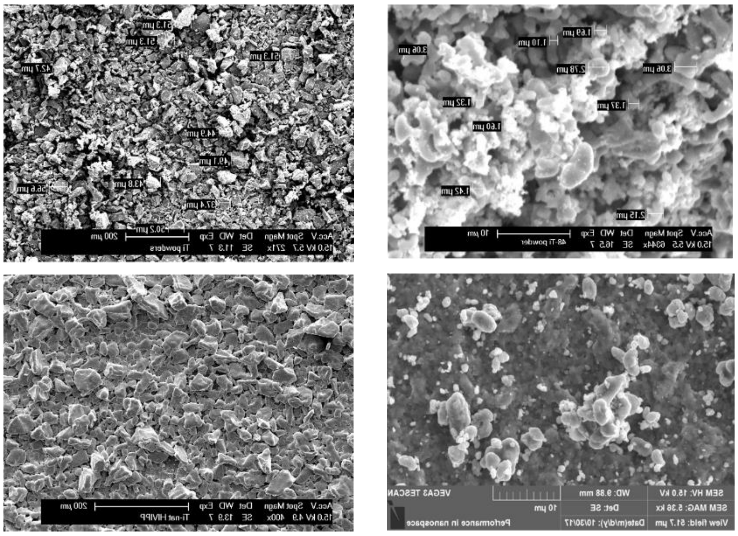

In collaboration with Valentino Rigato and Carlos Rossi Alvarez, the deposited target thicknesses were measured by using the Back-Scattering Rutherford method at the AN2000 accelerator at INFN-LNL. Figure 4 reports the results obtained with RBS analysis in case of the sample#25L (on the x-axis is reported the target profile); yellow dots represent experimental data, black dots the fitted data obtained by considering: the amount of Titanium atoms (red dots), Aluminium substrate (blue dots) and the Oxygen atoms (grey dots).

Figure 4. Results of RBS analysis

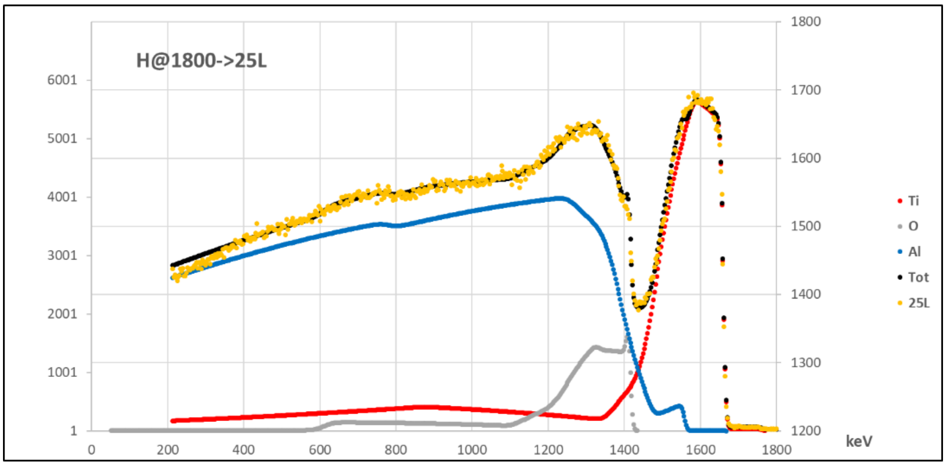

By using RBS technique a measurement of the deposit homogeneity was performed on two selected samples, showing that the deposit thickness was varying less than 10% on the entire surface (Figure 5).

Figure 5. Results of RBS analysis performed at INFN-LNL on ^{48}Ti metallic deposit on aluminum substrate

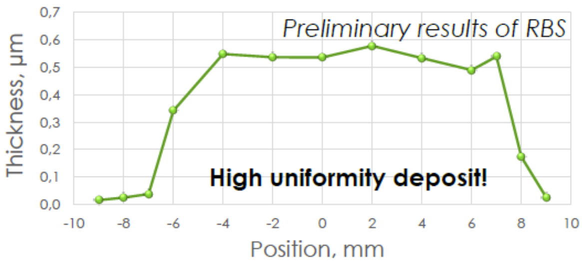

ENRICHED Ti-49 AND Ti-50 METALLIC POWDERS

During 2018 the enriched Ti-49 and Ti-50 metallic powders were purchased by the only supplier worldwide, to our knowledge, i.e. the Oak Ridge National Laboratories. The material received was not in the requested form of metallic powders, but in the form of metal sponge of different size and shape, up to 2 mm of grain size (Figure 6).

Figure 6. Enriched Ti-49 and Ti-50 purchased by Oak Ridge National Laboratories; metal sponges are visible

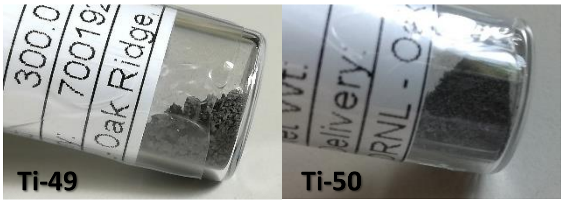

The HIVIPP method was tested with the smallest size grains of enriched ^{49}Ti (about 17 mg) to verify if the deposit was possible even with grains; Figure 7 reports the result and the SEM analysis on the obtained deposit.

Figure 7. Deposit of ^{49}Ti obtained by using the smallest grains of the enriched material; SEM analysis shows the presence of a big grain on the surface, that is not uniform

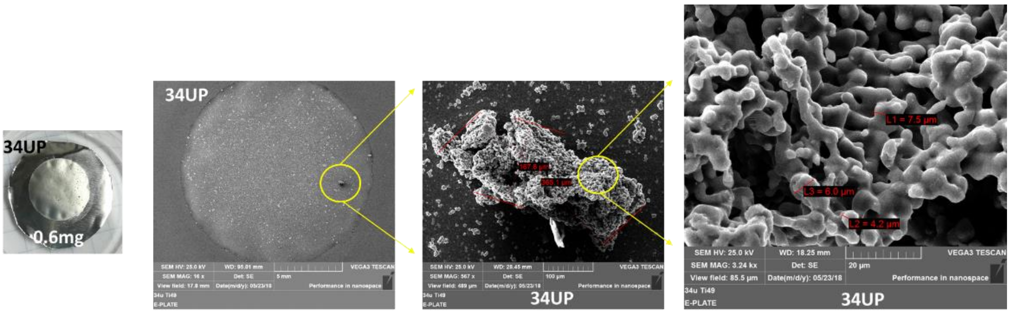

After this test, the idea of reducing the grains size was considered. First tests were done at INFN-LNL by using liquid nitrogen and a mortar; the enriched ^{49}Ti material remained after the deposition test was used; Figure 8 shows the obtained results.

Figure 8. Test with liquid nitrogen and mortar at INFN-LNL with remaining ^{49}Ti powder after deposition test

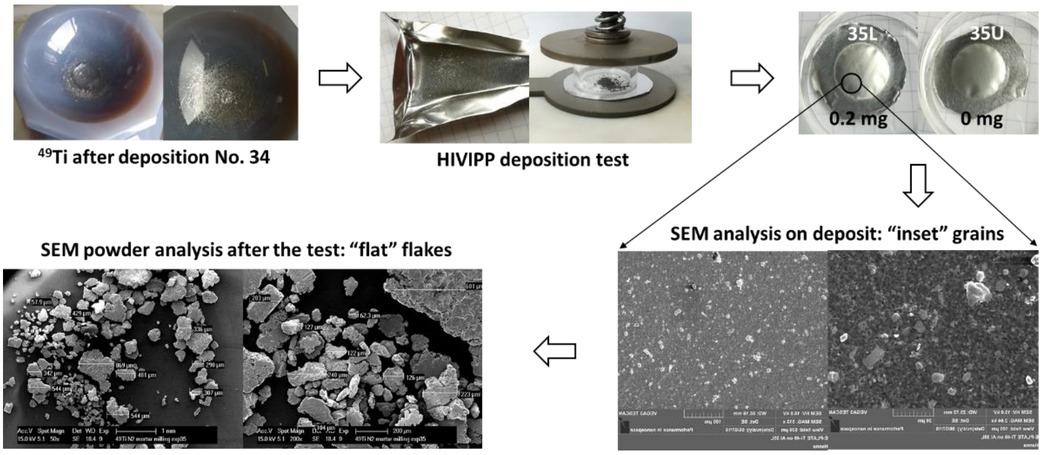

The positive outcome of this test (smallest flat grains were obtained) encouraged the use of a cryomill, that is able to apply a multidirectional effect on the powder, thanks to the mechanical and vibrational movement. Tests were done by using ^{nat}Ti metallic flakes and a commercial cryomill at the Verder Scientific headquarters; Figure 9 reports obtained results.

FIGURE 9. TEST WITH CRYOMILL AT VERDER SCIENTIFIC HEADQUARTERS WITH ^{NAT}TI METALLIC FLAKES AND GRANULOMETRIC ANALYSIS OF OBTAINED POWDER

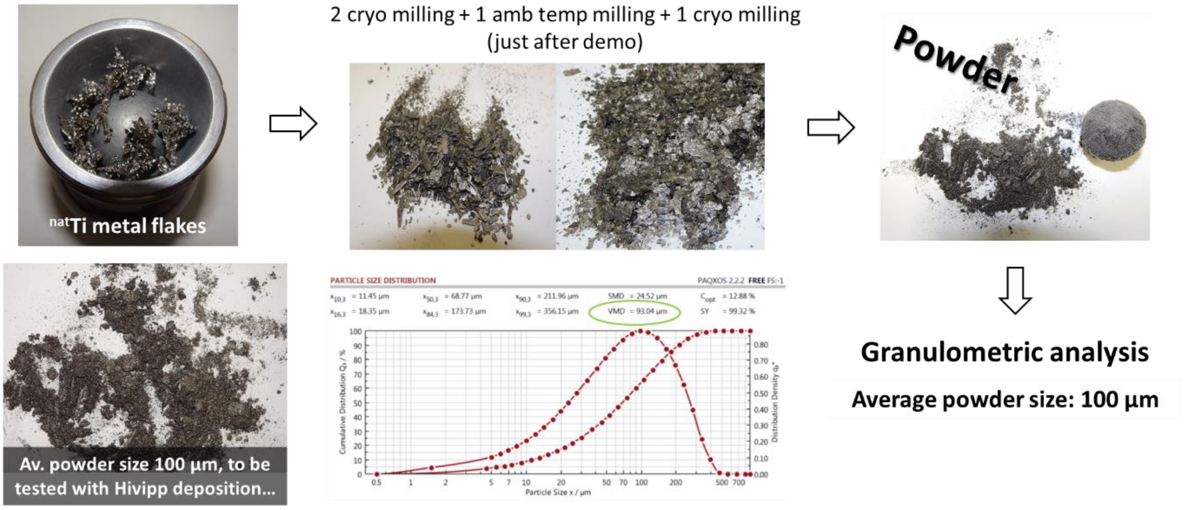

These positive results are the ground of the purchase of the cryomill, done with Laramed project funds. The cryomill was installed at INFN-LNL in October 2018; different tests were performed by using ^{nat}Ti metallic flakes to optimize the protocol before using the enriched powder; SEM analysis shows powder size ranging 5-70 µm diameter (Figure 10 and

Figure 11).

FIGURE 10. TEST WITH CRYOMILL AT INFN-LNL WITH ^{NAT}TI METALLIC FLAKES (VISUAL INSPECTION)

FIGURE 11. SEM ANALYSIS OF THE ^{NAT}TI METALLIC POWDER OBTAINED WITH THE TEST WITH CRYOMILL AT INFN-LNL

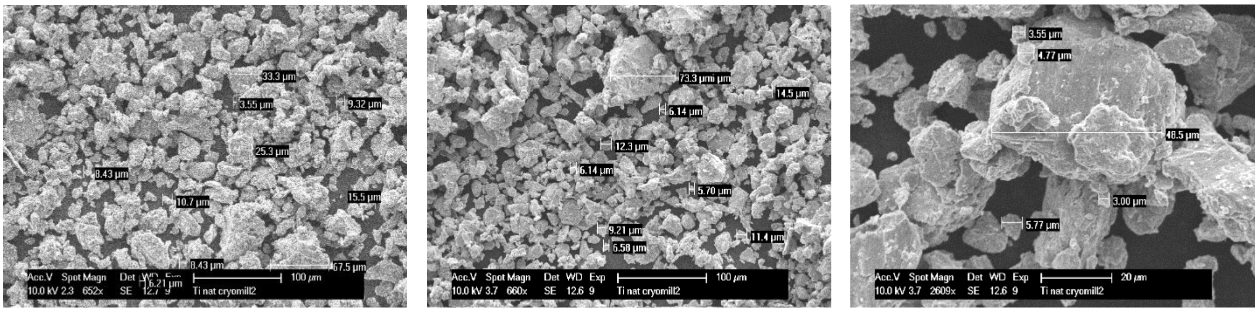

Additional tests are required in order to optimize the procedure, i.e. reduce the amount of lost material and eventual contamination.

➢ IRRADIATION RUNS AT THE ARRONAX FACILITY

During all the experiments performed at Arronax facility (**Figure 12**) the stacked-foils target technique was used, in order to obtained multiple measurements of the cross section at different energies during a unique irradiation run (**Figure 13**). **Table 1** reports the number of target foils inserted in the stacked-target and separated by aluminum foils, used as beam energy degrader.

In order to measure the proton beam current, a monitor foil was used and the recommended cross sections by IAEA were taken into account in data analysis (updated values, available from August 2017). Since the enriched metal targets of ^{48}Ti were not available before September 2017, the first three irradiation runs were dedicated to the measurement of the ^{nat}V(p,x)^{47}Sc nuclear reaction. This is a promising route for the production of ^{47}Sc for medical applications: in fact the co-production of isotopic impurities (such as ^{46}Sc) seemed to be reduced in comparison with other nuclear reactions and the target material is available in metal form and low price, since it is mainly composed by the V-51 isotope (99.75% abundance, V-50 0.25%). During the 4°, 5° and 6° irradiation run the enriched ^{48}Ti foils realized by HIVIPP method were used. Two deposits of ^{48}Ti on aluminum support were very thin (< 1 µm) and for this reason they were inserted in contact in the stacked-foils target structure used in the 4° run and considered as a unique target foil in data analysis.

FIGURE 12. PHOTOGRAPH OF THE ALIGNMENT PROCEDURE OF TARGET-HOLDER AND COLLIMATOR ON THE BEAM-LINE

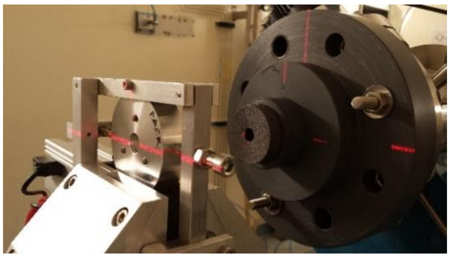

FIGURE 13. PHOTOGRAPH AND SCHEMATIC STRUCTURE OF THE STACKED-FOILS TARGET USED IN THE 4° IRRADIATION RUN

TABLE 1. DETAILS ON THE IRRADIATION RUNS PERFORMED AT ARRONAX FACILITY DURING THE PASTA PROJECT

Irradiation run	Date	Reaction	Target foils No.	Energy (MeV)	Duration (minutes)	Current (nA)
1	11/4/2017	$^{nat}V(p,x)^{47}Sc$	3	70.3	90	≈ 100
2	27/6/2017	$^{nat}V(p,x)^{47}Sc$	3	54.0	90	≈ 100
3	4/7/2017	$^{nat}V(p,x)^{47}Sc$	3	61.0	90	≈ 100
4	10/10/2017	$^{48}Ti(p,x)^{47}Sc$ $^{nat}V(p,x)^{47}Sc$	3* 3	34.0	90	≈ 120
5	22/11/2017	$^{48}Ti(p,x)^{47}Sc$ $^{nat}V(p,x)^{47}Sc$	4 1	40.0	50	≈ 130
6	17/04/2018	$^{48}Ti(p,x)^{47}Sc$ $^{nat}V(p,x)^{47}Sc$	3 1	34.0	90	≈ 100

➢ DATA ANALYSIS AND PRELIMINARY RESULTS

In order to follow the decay of the radionuclides of interest, it is necessary to perform ɣ-spectrometry measurements of the same sample at different times after the End Of Bombardment (EOB). At least No. 5 acquisitions of the same target foils were taken at each irradiation run; in particular, in order to measure the activity of the long-lived ^{46}Sc isotope (83.79 d half-life), all the target foils of each irradiation run were measured again during the first days of the following run.

Data analysis was performed considering the recent paper published by Otuka et al. (2017). All the produced radionuclides were taken into account, i.e. ^{47}Sc, ^{46}Sc, ^{44}Sc, ^{44m}Sc, ^{43}Sc, ^{48}Sc, ^{48}V, ^{43}K, ^{48}Cr, ^{49}Cr, ^{51}Cr. The cross section σ of the radionuclides of interest x is calculated considering the reference radioisotope r produced in the monitor foil and by using the following formula:

$$\sigma_x = \sigma_r \frac{C_x}{C_r}\frac{n_r}{n_x}\frac{\varepsilon_r}{\varepsilon_x}\frac{I_r}{I_x}\frac{f_r}{f_x}$$

Where σ_r is the reference cross section (available on IAEA website), C is the net number of counts of the ɣ-line considered, n is the number of target atoms/cm^2, ε is the detector efficiency at the energy of the ɣ-line considered, I is the intensity of the ɣ-line and f is the decay correction factor:

$$f_x = \left(1 - e^{-\lambda_x t_i}\right) e^{-\lambda_x t_{c,x}} \left(1 - e^{-\lambda_x t_{m,x}}\right)/\lambda$$

That takes into account the irradiation time t_i, the cooling time t_c from the EOB to the ɣ-spectrometry and the measuring time t_m.

Figure 14, Figure 15 and Figure 16 report some preliminary results obtained by irradiating ^{nat}V targets with proton beams up to 70 MeV.

N. Otuka et al., *Uncertainty propagation in activation cross section measurements*, Radiation Physics and Chemistry 140 (2017) 502-510

FIGURE 14. PRELIMINARY RESULTS OF THE ^{NAT}V(P,X)^{47}SC,^{46}SC NUCLEAR CROSS SECTIONS

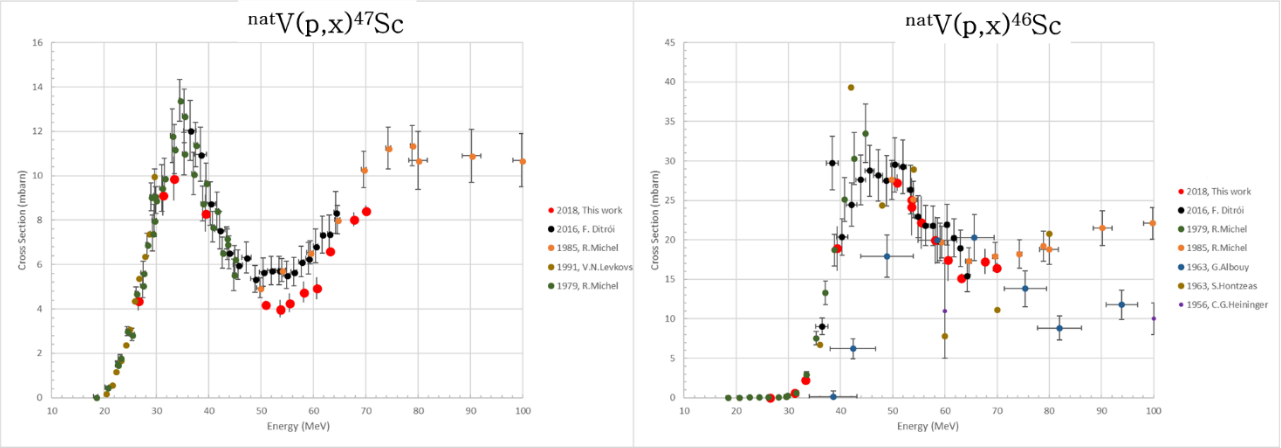

FIGURE 15. PRELIMINARY RESULTS OF THE ^{NAT}V(P,X)^{44}SC,^{44M}SC,^{48}SC,^{48}V, ^{43}SC,^{43}K NUCLEAR CROSS SECTIONS

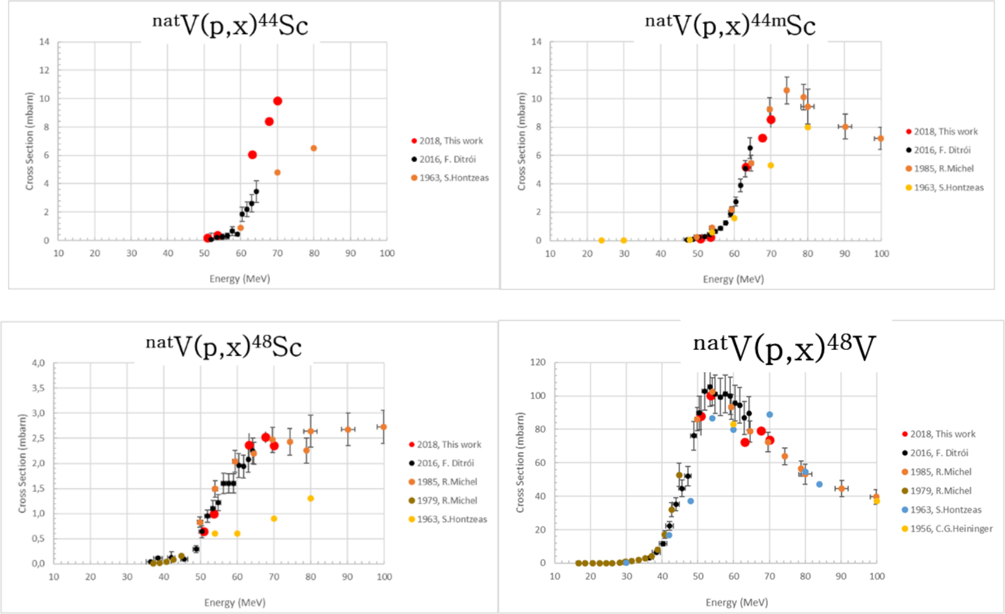

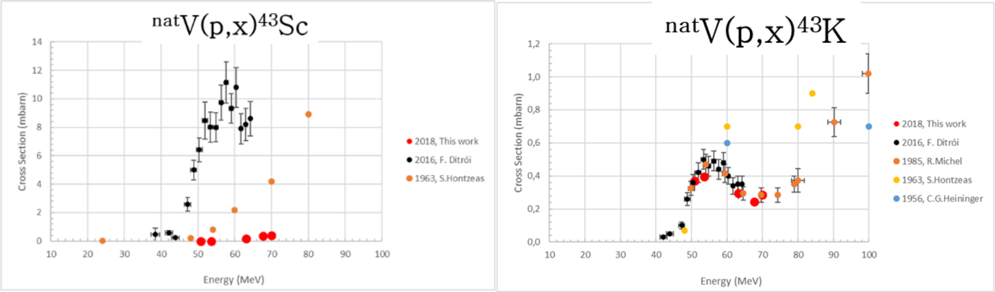

Figure 16. Preliminary results of the ^{nat}V(p,x)^{48}Cr,^{49}Cr,^{51}Cr nuclear cross sections

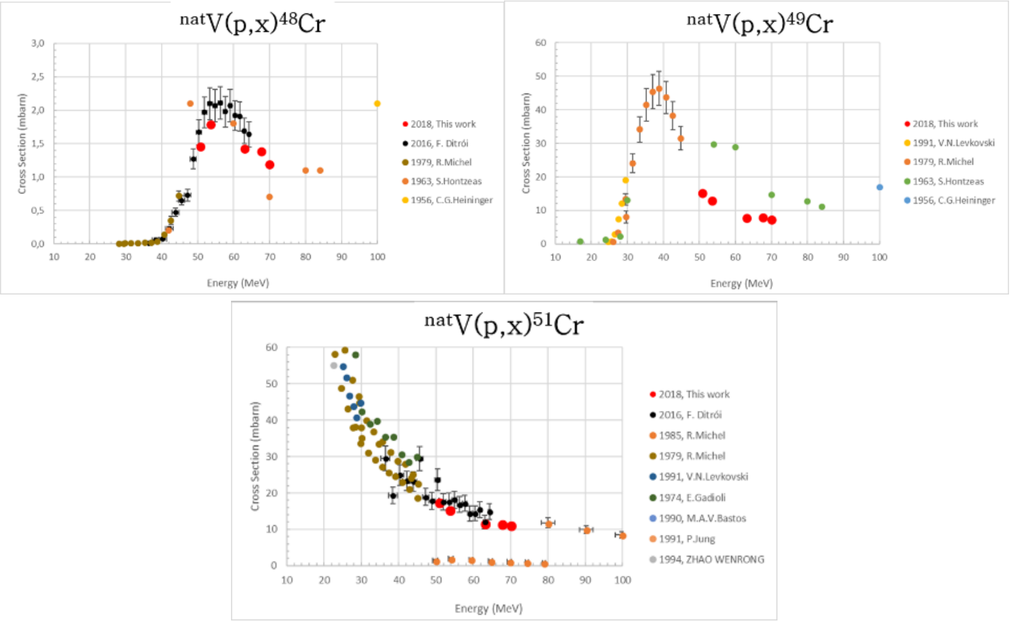

➢ THEORETICAL STUDIES ON NUCLEAR CROSS SECTIONS

We have calculated production of the theranostic ^{47}Sc by proton collision with targets of ^{nat}Ti, ^{48}Ti, ^{49}Ti, ^{50}Ti and ^{nat}V. Analysis has been performed with nuclear reaction codes Talys 1.9, Empire 3.2 and Fluka development version 2018.0. The gray band shown in the following graphs has been created with the variety of TALYS calculations considered with different preequilibrium and level-density models: 24 different results ranging from a maximum to a minimum are shown in Figure 18, Figure 21 and Figure 22.

Considering the co-production of Sc-isotopes that may affect the radionuclidic purity of ^{47}Sc (^{46}Sc is the radionuclide of major concern since it has a longer half-life than ^{47}Sc), in the following graphs is also shown the ratio of the cross sections for ^{47}Sc/Sc-isotopes production, in order to identify the best energy region, i.e. the interval where the production of ^{47}Sc is maximized. From this analysis, it resulted that the use of ^{nat}Ti and ^{48}Ti targets (73.72% natural abundance) appears not suitable for the production of ^{47}Sc with high purity, since up to 100 MeV there is no energy region where ^{47}Sc is produced with no contamination (Figure 17 and Figure 18).

Figure 17. Theoretical estimations of the ^{nat}Ti(p,x)^{47}Sc,^{46}Sc cross sections (upper graphs) and ^{47}Sc/all-Sc-isotopes cross section ratio (lower graphs); no interesting energy region for ^{47}Sc production can be identified

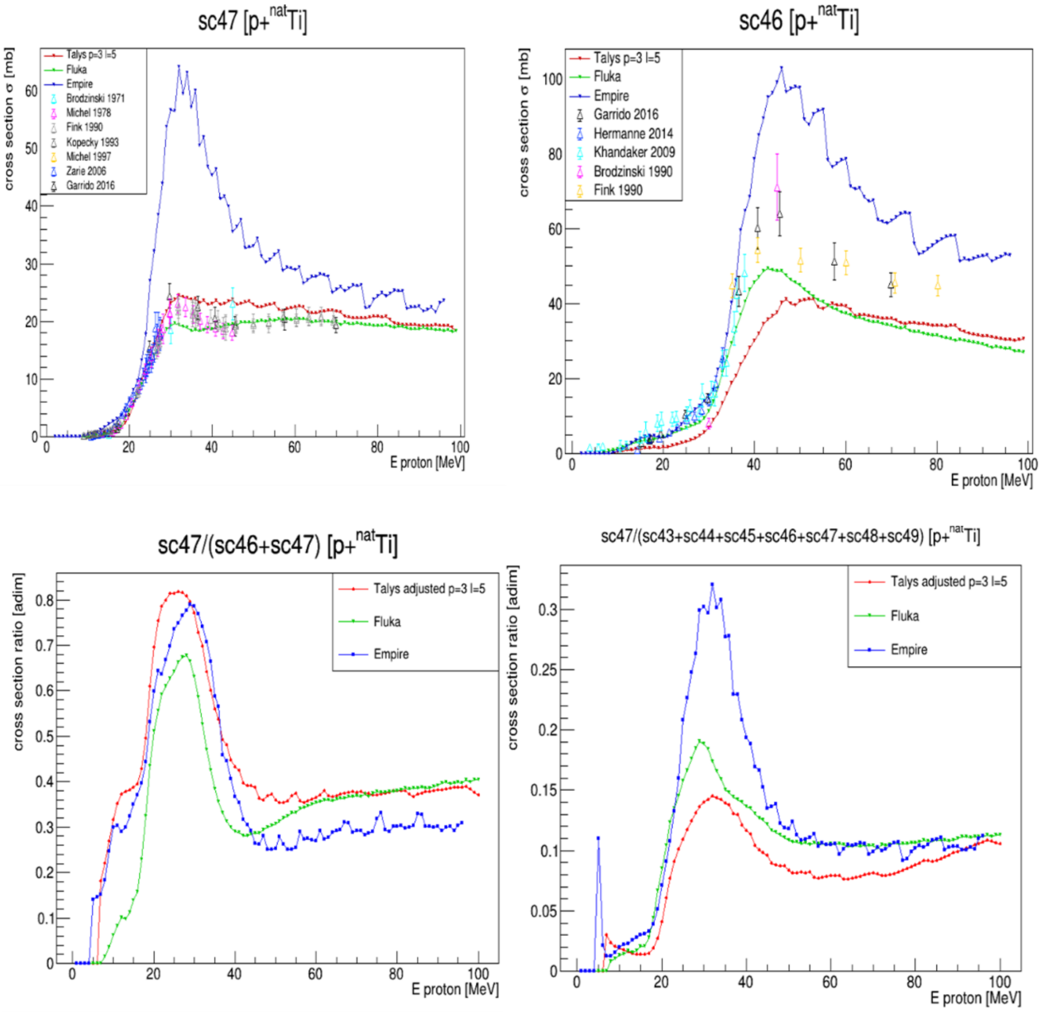

Figure 18. Theoretical estimations of the ^{48}Ti(p,x)^{47}Sc,^{46}Sc cross sections (upper graphs) and ^{47}Sc/all-Sc-isotopes cross section ratio (lower graphs); no interesting energy region for ^{47}Sc production can be identified

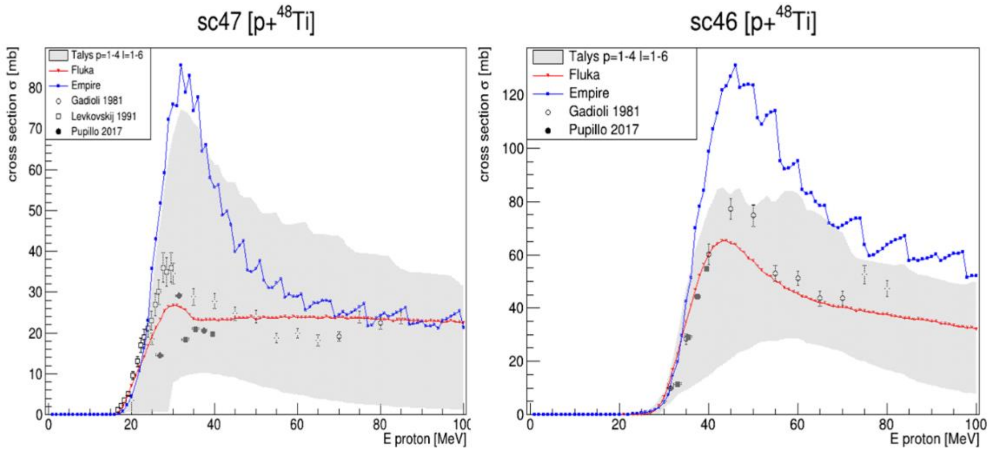

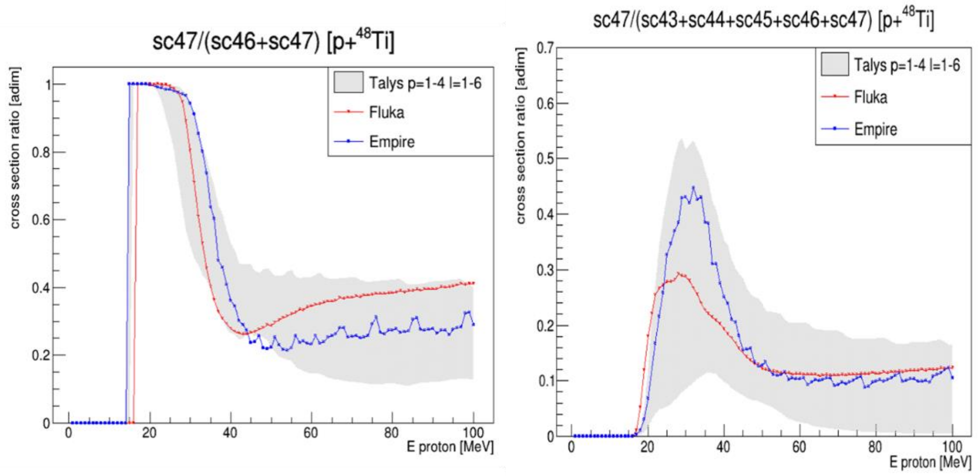

On the contrary, by using targets of ^{49}Ti (5.41% natural abundance), ^{50}Ti (5.18% natural abundance) and ^{nat}V, it is possible to identify energy regions suitable for the production of ^{47}Sc.

The selected energy regions for ^{47}Sc production are:

- 25-40 MeV for the enriched ^{49}Ti target (**Figure 19**),
- 10-20 MeV for the enriched ^{50}Ti target (**Figure 20**),
- 20-30 MeV for the ^{nat}V target (**Figure 21**).

In case of the ^{50}Ti target the calculation with Talys code has been performed by the model suggested by Duchemin et al. (2015), while for ^{nat}V we have varied both the preequilibrium model (preeqmode ranging 1-4) and the level-density model (ldmodel ranging 1-6), producing the grey band shown in the plots.

It has to be noted that in case of the ^{nat}V target (mainly composed by ^{51}V with 99.75% natural abundance), the production of ^{46}Sc for E_P < 25 MeV is due to the 0.25% of ^{50}V in the ^{nat}V target, as shown in **Figure 22**.

C. Duchemin et al., Phys. Med. Biol. 60 (2015) 931-946

Figure 19. Theoretical estimations of the ^{49}Ti(p,x)^{47}Sc, ^{46}Sc cross sections (upper graphs) and ^{47}Sc/all-Sc-isotopes cross section ratio (lower graphs); the best range for ^{47}Sc production is 25-40 MeV

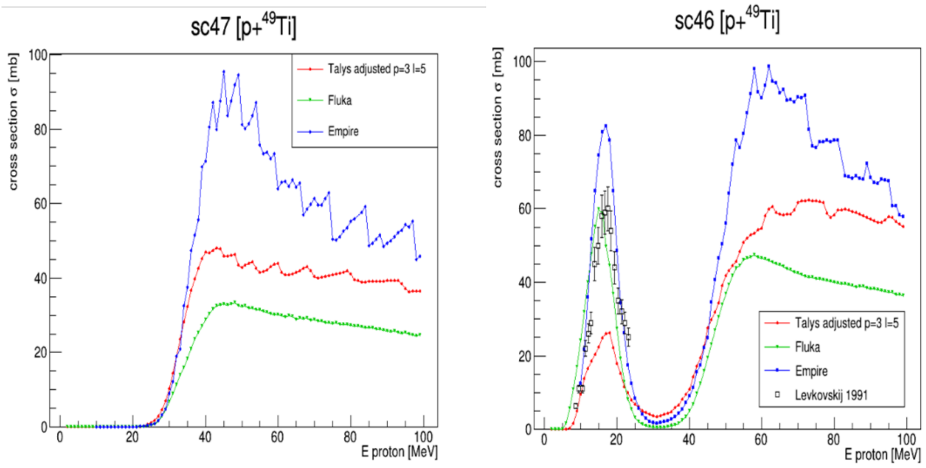

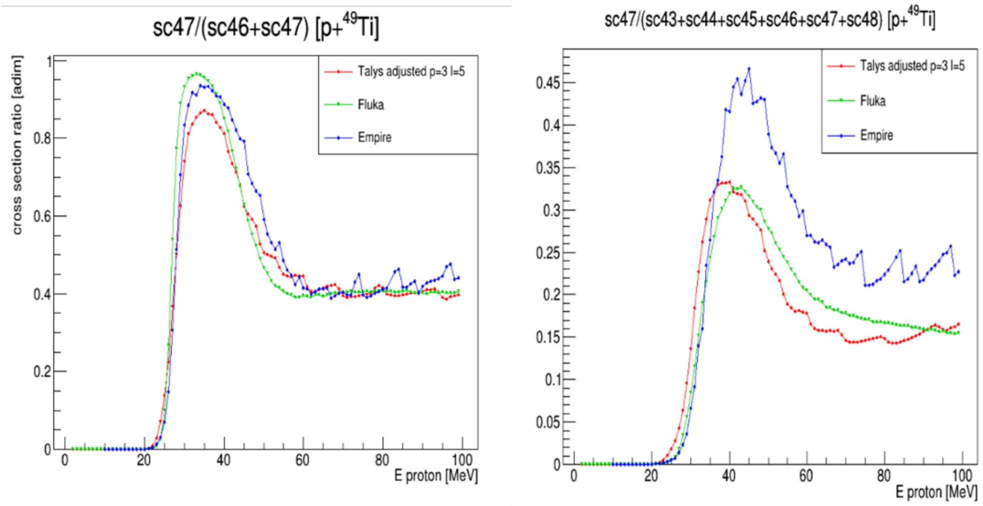

Figure 20. Theoretical estimations of the ^{50}Ti(p,x)^{47}Sc, ^{46}Sc cross sections (upper graphs) and ^{47}Sc/all-Sc-isotopes cross section ratio (lower graphs); the best range for ^{47}Sc production is 10–20 MeV

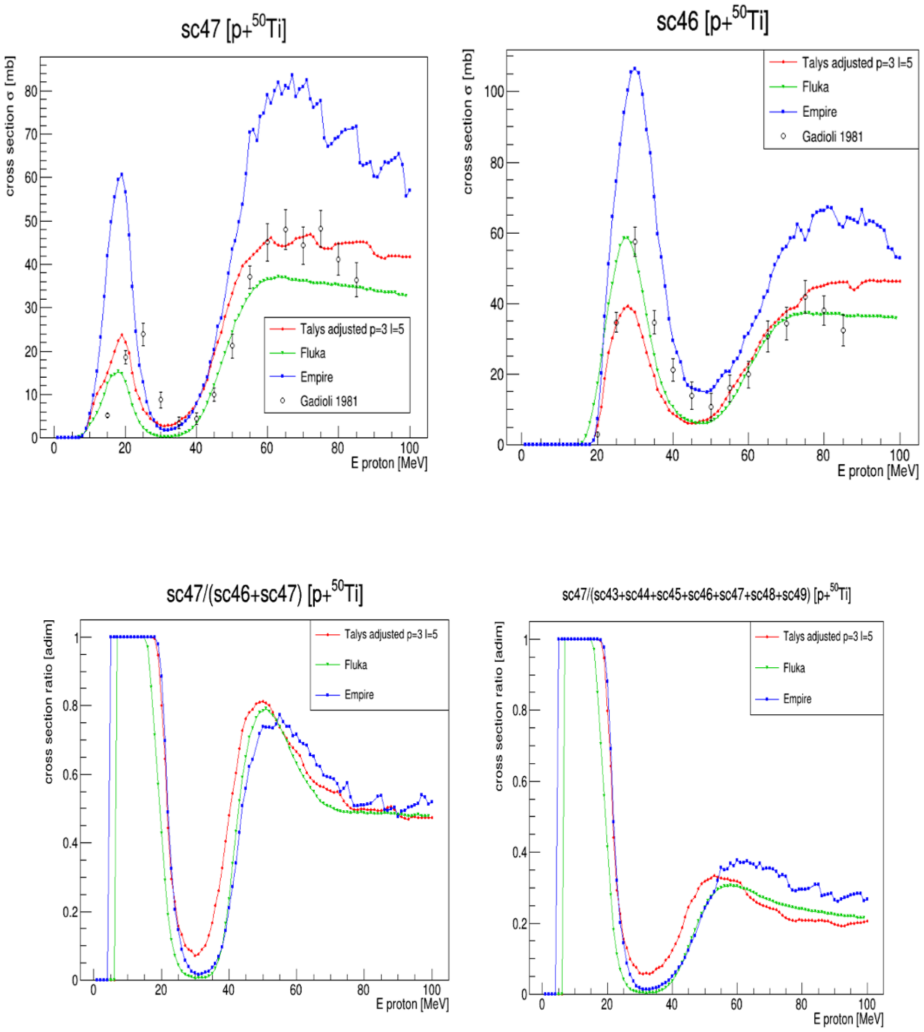

Figure 21. Theoretical estimations of the ^{nat}V(p,x)^{47}Sc, ^{46}Sc cross sections (upper graphs) and ^{47}Sc/all-Sc-isotopes cross section ratio (lower graphs); the best range for ^{47}Sc production is 20–30 MeV

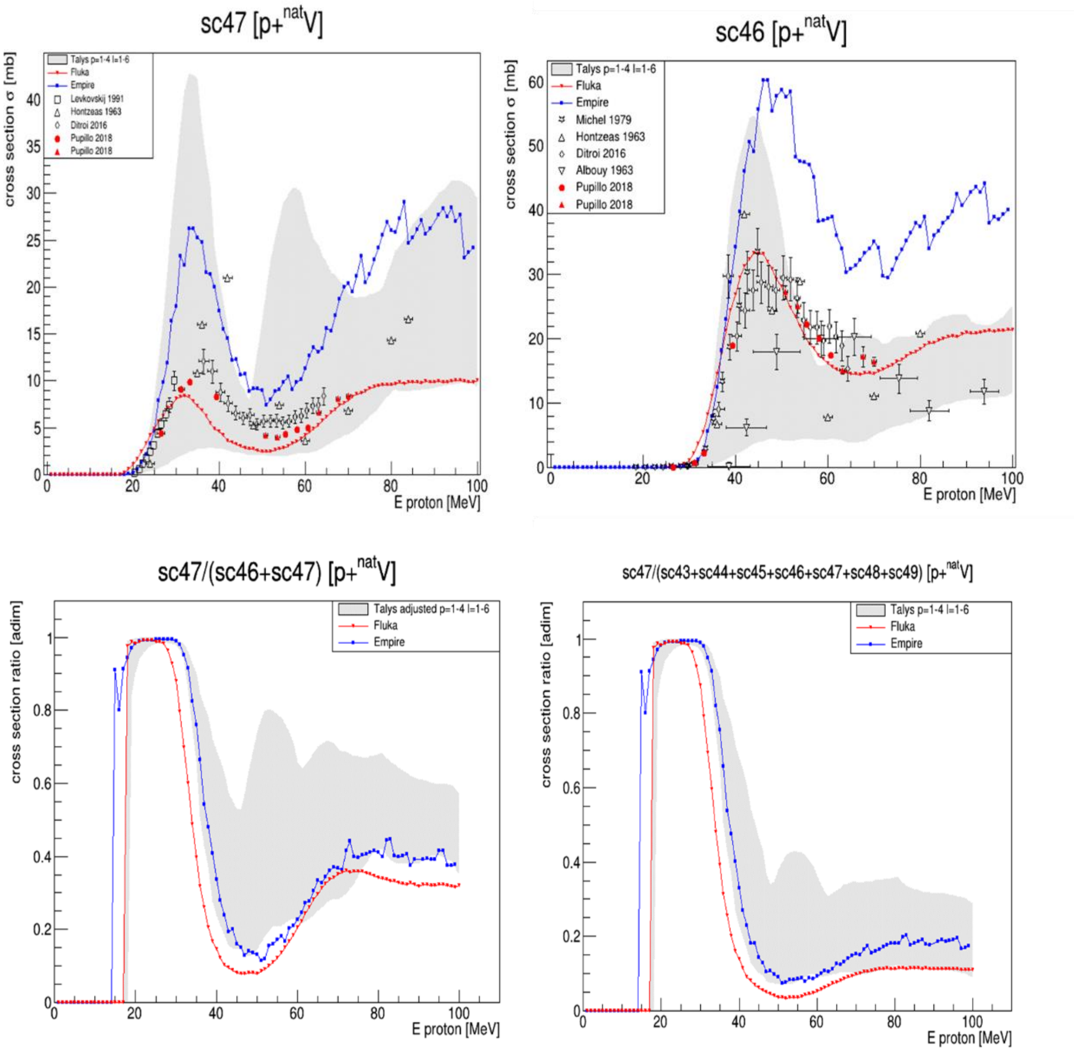

FIGURE 22. THEORETICAL ESTIMATIONS OF THE ^{50}V(P,X)^{46}SC (LEFT) AND ^{51}V(P,X)^{46}SC (RIGHT) CROSS SECTIONS

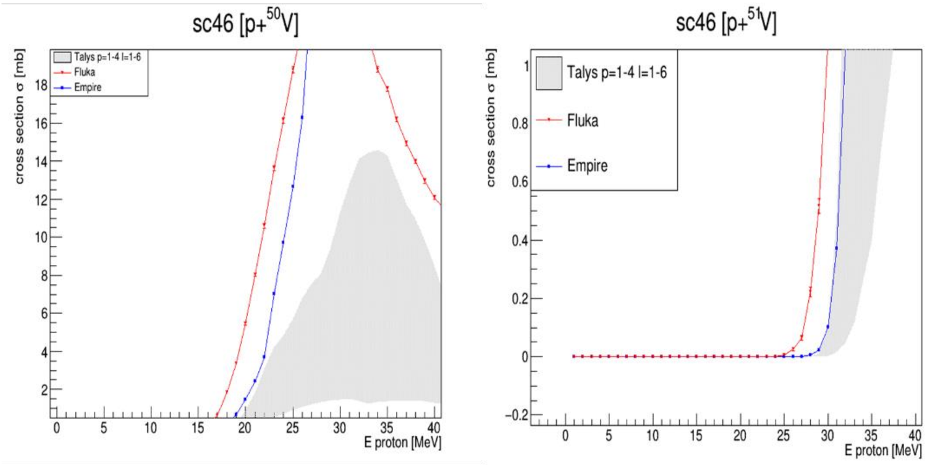

THICK TARGET YIELD CALCULATIONS WITH V-nat

For natural vanadium targets we have calculated the activity produced assuming a 300 µA proton beam with incident/outgoing energy E_{in}=29 and E_{out}=24 MeV respectively, corresponding to a target thickness of 600 µm. In the case of Talys calculations the available models provide a band of results, going from a maximum and a minimum activity value, as shown in **Figure 23**. Assuming 1 h of irradiation we get at EOB a maximum of 1.04 GBq and a minimum of 56.32 MBq for ^{47}Sc, and a coproduction of ^{46}Sc ranging from 50.69 kBq (max) to 8.28 kBq (min), as shown in **Table 2** and **Figure 23**. The Talys models that are in best agreement with experimental data provides a ^{47}Sc activity at EOB of 275.63 MBq and a ^{46}Sc activity of 23.55 kBq.

TABLE 2. THEORETICAL ESTIMATIONS OF ^{47}SC AND ^{46}SC ACTIVITY VALUES CALCULATED BY USING THICK ^{NAT}V TARGETS

Time	^{47}Sc Act. min	^{47}Sc Act. max	^{46}Sc Act. min	^{46}Sc Act. max
EOB	56.32 MBq	1.045 GBq	8.28 kBq	50.69 kBq
9 h after EOB	52.11 MBq	0.97 GBq	8.26 kBq	50.54 kBq

It is important to note that in the following graphs (Figure 23, Figure 24 and**Errore. L'origine riferimento non è stata trovata.**) the time scale starts at the beginning of the bombardment and that the same irradiation parameters are considered: target ^{nat}V, T_{IRR} = 1h, E_P= 29-24 MeV, I_P = 300 µA.

FIGURE 23. THEORETICAL ESTIMATIONS OF ^{47}SC AND ^{46}SC ACTIVITY VALUES VS TIME (T_0 IS START OF THE IRRADIATION)

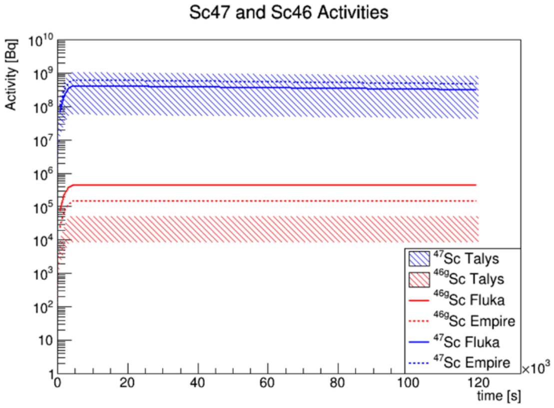

On the left-hand side (l. h. s.) of **Figure 24** we illustrate the time evolution of the Isotopic Purity of ^{47}Sc for the first 35000 s, where t=0 defines the start of bombarding and the irradiation time is t_{IRR}=3600 s. On the right-hand side (r. h. s.) we illustrate a similar time evolution for the radionuclidic purity (RNP). The calculation refers to different reaction codes TALYS, EMPIRE, FLUKA and compares the corresponding results.

Figure 25 refers to the RNP calculated only with TALYS code, using an optimal choice of parameters, and describes a period of more than 40 days, which clearly exhibits the decline of the RNP due to the much longer half-life of ^{46}Sc compared to ^{47}Sc. It must be noted also that the time evolution of RNP shown in **Figure 24** r. h. s. differs from that of **Figure 25** because in the panel of **Figure 25** it was possible to consider also the contribution of the metastable state ^{46m}Sc. The contribution of metastable states could be included only with TALYS calculations, while with EMPIRE and FLUKA it was not considered. For this reason, we showed on the r. h. s of **Figure 24** the time evolution of the RNP comparing the results of the three different nuclear reaction codes, without the inclusion of the contribution of the ^{46m}Sc state in all the calculations, so the three curves could be compared on equal footing.

These results appear very promising and should stimulate thick target yield (TTY) measurements in the corresponding energy range.

Figure 24. Theoretical estimations of ^{47}Sc Isotopic (left) and RadioNuclidic Purity (right) vs time by using the irradiation parameters: target ^{NAT}V, T_{IRR} = 1h, E_P= 29-24 MeV, I_P = 300 µA

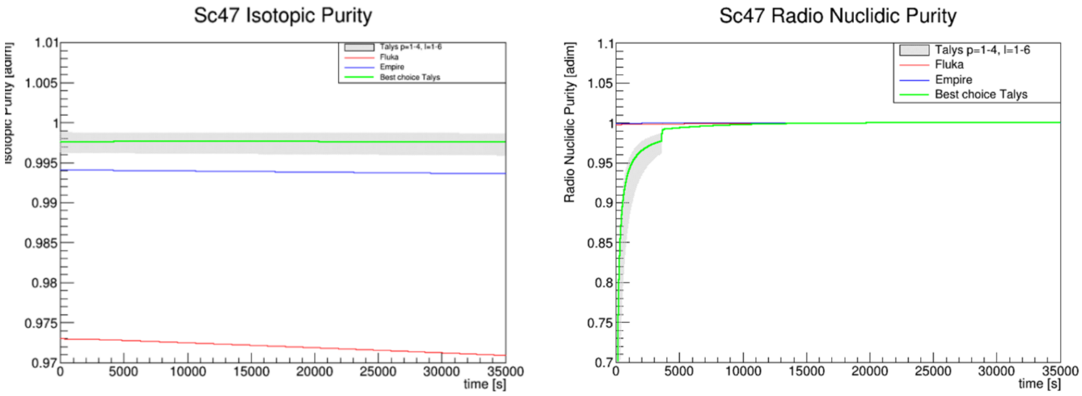

Figure 25. Theoretical estimation of ^{47}Sc Radionuclidic Purity vs time about 3 weeks after EOB by using the same irradiation parameters and the Best choice Talys

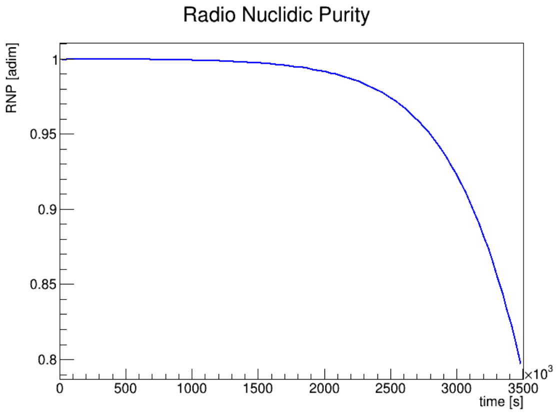

➢ RADIOCHEMISTRY

Considering the medical application of cyclotron-produced ^{47}Sc, the development of a target processing to extract the desired product in an injectable form is mandatory. The process should accomplish the separation in a high yield of ^{47}Sc from the Ti bulky metal target and the purification of the isolated product from others trace stable/unstable contaminants and solvents. Moreover, the procedure time should be minimized to reduce as much as possible the decay loss.

Within this project, we have set ourselves the goal of developing a dissolution/separation/purification procedure for the production of Sc isotopes from titanium metal targets and to identify the proper dissolution condition of vanadium metal targets for spectrometry analysis purposes.

The very first step of a separation procedure applied to a solid target is the target dissolution and eventual conversion of the solutes into a chemical form suitable for the separation (e.g. formation of the cationic or anionic complex). The dissolution step optimization strictly depends on target characteristics (e.g. composition, mass, thickness, deposition method etc). The chemical study started by considering an amount of titanium mass (of the order of dozens mg) in view of scaling up the procedure (dissolution and separation methods) once defined the proper titanium target configuration (mass, thickness, surface, enrichment, chemical purity etc.).

The dissolution step in case of metal titanium is very challenging since this material is known to be physically inert to most acids at room temperature. The majority of literature data reports dissolution/separation procedures for Sc production from titanium dioxide targets (TiO_2) and only one paper, according to our knowledge, reports scandium production from titanium in metal form. In all cases, hydrofluoric acid (HF) has been used for the dissolution and separation process. Considering the toxicity of the fluoride anion and the difficulties related to the use of HF, some dissolution tests were performed by using different solvents to find out an alternative to hydrofluoric acid employment.

In the case of vanadium metal targets, the dissolution is easier and achievable even at room temperature with medium/low concentrated acid solutions.

It is important to choose the dissolution step considering also the following separation method that has to be applied. After a deep evaluation of the literature on separation and purification of Sc from Ti and the chemical properties of the resins purchased, we performed radiochemical separation tests to find out the best separation and purification procedure to obtain an injectable product.

Objectives of radiochemistry:

- To determine a post irradiation dissolution procedure for thick Vanadium targets
- To determine a post irradiation dissolution procedure for Titanium metal targets avoiding hydrofluoric acid solvent
- To develop a radiochemical procedure for the separation and purification of Sc isotopes from a titanium target

DISSOLUTION OF V-nat

- *Preliminary tests with thin vanadium targets*

With the aim to identify the best dissolution condition for dissolving vanadium targets in 5 ml spectrometry vials we performed five dissolution tests of thin vanadium metal foil (20 µm, purity 99.8%) with different solvents as summarized in Table 3.

TABLE 3. PRELIMINARY DISSOLUTION TESTS OF V METAL THIN FOILS

Test #	Mass (mg)	Solvent	Volume (mL)	Dissolution time	Note
1	14	HNO_3 15M	5	15 min	Violent
2	14	HNO_3 7M	5	20 min	

3	15	Aqua regia	5	2 h	Dark turbid
4	14	HNO_3 4M	5	over 1 day	
5	**14**	**HNO_3 7M**	**2.15**	**20 min**	**Diluted up to 5ml with distilled H_2O**

On this regard, we decided to avoid the use of HNO_3 15M for the strength and violent reaction.

We preferred to use HNO_3 7M over aqua regia and HNO_3 4M because slightly more active and faster than the latter. In particular, the dissolution test performed with aqua regia brought to a dark and turbid solution at first and took over 2 h to get a clear limpid solution.

Since a complete dissolution occurs even at a lower volume of HNO_3 7M, in order to minimize the acid concentration involved we select #5 as best dissolution condition.

- *Thick V target dissolution tests*

We performed seven dissolution tests of thick vanadium metal foil (0.5 mm, purity 99.8%) with HNO_3 at different concentration and volumes as summarized in Table 4.

TABLE 4. THICK VANADIUM TARGET DISSOLUTION TESTS

Test #	Mass (g)	Solvent	Volume (ml)	Note	Result
1	0.35	HNO_3 7M	1.5	In spectrometry vial Violent reaction	Not dissolved
2	0.34	HNO_3 1M	5	In spectrometry vial no reaction	Not dissolved
3	0.34	HNO_3 2M	5	In spectrometry vial no reaction	Not dissolved
4	0.36	HNO_3 4M	2.5	In spectrometry vial Violent reaction	Not dissolved
5	**0.35**	**HNO_3 4M**	**30**	**In glass flask**	**Dissolved**
6	0.35	HNO_3 2M	30	In glass flask	Not dissolved
7	0.37	HNO_3 3M	30	In glass flask	Not dissolved

Dissolution tests of samples from 1 to 4 have been performed in 5 ml spectrometry vials; due to the high vanadium mass and small volume available the dissolution in this condition of an irradiated target it is impracticable, as shown in Figure 26 (a) and (b). The violent reaction cannot be confined in such a small volume and if trying to minimize the acid concentration the dissolution does not occur at all. In light of this result, we decided to perform the dissolution in a glass flask with 30 ml of HNO_3 4M, as shown in Figure 26 (c); the complete dissolution occurred in 4h.

Figure 26. Photographs of dissolution tests of thick ^{nat}V target: sample#1 (a), sample#4 (b) and sample#5 (c)

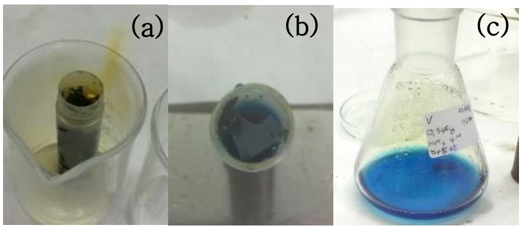

- *Dissolution procedure to be applied in experimental condition at ARRONAX*

From the results described above, we defined a dissolution procedure to be applied to irradiated vanadium thick targets at ARRONAX facility. The list of materials used and the step-by-step procedure is hereafter described.

Materials

- ^{nat}V (thickness=0.5 mm, mass ~ 350 mg)
- 30 ml HNO_3 4M (8 ml HNO_3 ~70% + 22 ml H_20 milliQ) + 5 or 10 ml extra (40 ml total = 10.5 ml HNO_3+ 29.3 ml H_2O)
- Pyrex/glass bottle 80 ml (or more) with blue caps
- Mechanical vortex

Methods

1. Weight the empty glass bottle with the blue cap
2. Insert the irradiated V target into the glass bottle
3. By means of a plastic Pasteur, add slowly the 30 ml of HNO_3 4M to the bottle with V-target
4. Place at the top of the bottle the blue cap without screwing it
5. From time to time, check the dissolution trend and take off the cap for few seconds
6. If the V-target is not dissolved in few hours, add 5 ml more of HNO_3 4M
7. The day after check if the target is dissolved
8. If not, add 5ml more of HNO_3 4M
9. When the V-target is completely dissolved, screw the blue cap, weight the bottle with the V-solution
10. Vortex the solution before aliquoting
11. With a P5000 pipette, withdraws 5 ml of V-solution and put it in a spectrometry vial (previously weighted)
12. Weight the spectrometry vial filled with V-sol aliquot

DISSOLUTION TESTS OF METALLIC TITANIUM TARGETS

With the aim to identify the best dissolution condition for dissolving titanium targets, avoiding the use of hydrofluoric acid (HF), we performed several dissolution tests of titanium metal foil with different solvents and different HCl concentrations, as summarized in Table 5. First of all, we tested different solvents and solvent mixtures (as described in the previous project report PASTA-2017) to identify the best solvent. Tests were performed on metallic natural titanium samples (purity 99.6%; thickness 0.125 mm; mass 12.0 ± 1.7 mg) by heating at 100°C for 4 hours and then let the solution react overnight.

Table 5. Solvents and solvent mixtures employed in the preliminary dissolution experiments of metallic titanium samples and eventual intermediate heating applied to the sample before adding the second solvent.

Test #	solvent#1 Type and conc.	volumes# 1 (ml)	Interm. Heating (°C)	interm. heating time (min)	solvent#2 Type and conc.	volumes# 2 (ml)	Result
1	NaOH 6M	5					not dissolved
2	H_2O_2 30%	5					not dissolved
3	**HCl 12M**	**5**					**dissolved**
4	HCl 6M	5					not dissolved
5	**HCl 9M**	**5**					**dissolved**
6	NaOH 6M	4			H_2O_2 30%	1	not dissolved
7	HCl 12M	4	100	15	H_2O_2 30%	1	not dissolved
8	HCl 12M	1	100	15	H_2O_2 30%	4	not dissolved
9	HCl 12M	2.5	100	15	H_2O_2 30%	2,5	not dissolved
10	H_2O_2 30%	1	100	15	HCl 12M	4	not dissolved
11	H_2O_2 30%	4	100	15	HCl 12M	1	not dissolved
12	H_2O_2 30%	2,5	100	15	HCl 12M	2,5	not dissolved
13	**NaOH 6M**	**4**	**100**	**15**	**H_2O_2 30%**	**1**	**dissolved**
14	NaOH 6M	1	100	15	H_2O_2 30%	4	not dissolved

15	NaOH 6M	2,5	100	15	H_2O_2 30%	2,5	dissolved
16	HCl 12M	4			H_2O_2 30%	1	not dissolved
17	KOH 6M	5					not dissolved
18	NaOH 8M	5					not dissolved

As described in Table 5, only four samples were completely dissolved overnight, in particular when using highly concentrated hydrochloric acid (12 or 9 M) and a mixture of sodium hydroxide and hydrogen peroxide in the different ratio (4:1 and 1:1).

In respect to the separation and purification procedure selected to be investigated (Solid Phase Extraction chromatography), we choose HCl as solvent for further dissolution tests. As summarized in Table 6, thin titanium samples (20 µm, purity 99.6%) have been dissolved in different HCl concentration and volumes; HCl has been added to all samples one ml at a time at intervals of 15-30 min.

Table 6. Titanium dissolution test with HCl at different concentration and volumes (RT= room temperature)

Test #	Mass (mg)	HCl conc (M)	Volume (ml)	Dissolution time	Note
1	14.5	12M	2	15 min (100°C) + 45 min RT	
2	14	12M	2	15 min (100°C) + 45 min RT	
3	10	6M	2	15 min (100°C) + 45 min RT + 30 min (100°C)	
4	10.1	6M	2	55 min (100°C)	
5	10.2	4M	3	60 min (100°C)	
6	9.9	3M	3	75 min (100°C)	
7	10	2M	5	120 min (100°C)	
8	10.1	1M	>5	>4 h (100°C)	Not dissolved
9	9.7	12 M	5	165 min (100°C)	0.125 mm thick

All samples, except for #8, were successfully dissolved at HCl concentrations higher than 1M at 100°C in a reasonable time (1-2 hours); Figure 27 shows the results obtained with sample #5. We verified also the dissolution of a thick target (0.125 mm, purity= 99.6%, sample #9) in HCl 12 M to ensure the applicability of the procedure to thicker targets in view of a production scale up.

Figure 27. Photographs of sample#5 before (left) and after (right) the dissolution test

Sc/Ti SEPARATION AND PURIFICATION PROCEDURE

Recently some procedures have been developed to separate ^{43}Sc from ^{46}Ti using a DGA extraction chromatographic resin, as reported by Domnanich et al. (2017). This resin selectively retains Sc, leaving Ti to flow through the resin, in a 4M HCl solution. Pourmand et al. 2010 also reported the strong Sc(III) retention on DGA resin and the negligible Ti(III) retention at HCl molarities below 6 M.

Starting from the literature outcomes we have investigated a separation and purification procedure based on DGA-N extraction chromatographic resin (normal, particle size 50-100 µm, TrisKem International, Bruz, France).

The radiochemical separation has been developed with cold materials (non-radioactive) by simulating the real experimental conditions after the irradiation. The efficiency of the procedure has been evaluated by ICP-OES analytical analysis quantifying element trace in all the solutions. To perform our tests, we always prepared a mock solution by dissolving 10 mg of natural metallic titanium (thickness=20 µm, purity=99.6%) in 3 ml of HCl 4M and adding 2 µl of a 1000 mg/l scandium standard solution in HNO$_3$ (5%). Briefly, 85 mg of DGA resin was packed in a 1 ml column and conditioned with 5 ml of HCl 4M; the mock solution, containing Ti and Sc, was loaded on the resin, the Sc was retained while the Ti was eluted off and collected in the first sample called LOAD; the resin was then washed with 5 ml of HCl 4M to ensure complete removal of Ti(III) and collected in the sample called WASH; finally, the Sc (III) was eluted from the resin with 4 ml of HCl 0.1M and collected in the sample called ELUTION. Several tests have been conducted to select the proper eluent (water, saline, HCl) and volume.

Aiming to maximize the Sc/Ti separation yield and concentrate the final product in compatible solution with radiolabeling procedures, the eluted scandium solution (4 ml of HCl 0.1M) was rinsed with 1.5 ml of concentrated HCl to get an HCl solution at molarity around 2.5-3. The solution was loaded onto a second 1 ml column cartridge, containing ~30 mg DGA-N and after washing with 5.0 ml of 2.5M HCl, Sc(III) was eluted with 0.7 ml of water. All eluted fractions were analyzed by ICP-OES (Optima 3100 XL, Perkin Elmer, wavelengths: Ti = 336.121 nm; Sc = 361.383 nm). Table 7 summaries the experiments and separation efficiency achieved, resulting by ICP-OES analysis.

Table 7. Summary of the separation tests performed and their efficiency. (DL) detection limit:

DL (Sc) = 40 ppb; DL* (Ti) = 0.2 ppm

Test	Sample	Eluent	Vol (ml)	Ti (ppm)	Sc (µg)

#1	LOAD	HCl 4M	5		< DL
	WASH	HCl 4M	5		< DL
	ELUITION	HCl 0.1M	4	1.06	2,144
#2	LOAD	HCl 4M	2		< DL
	WASH	HCl 4M	5		< DL
	ELUITION	HCl 0.1M	4	0.69	2.376
#3	LOAD	HCl 4M	1.5		< DL
	WASH	HCl 4M	6		< DL
	ELUITION	HCl 0.1M	4	2.81	2.88
#4	LOAD	HCl 4M	1.5		< DL
	WASH	HCl 4M	6		< DL
	ELUITION	water	4	3.44	2.7
#5	LOAD	HCl 4M	1.5		< DL
	WASH	HCl 4M	6		< DL
	ELUITION	saline	4	9.1	2.18
#6	LOAD1	HCl 4M	1.5		< DL
	WASH 1	HCl 4M	6		< DL
	LOAD2	HCl 2.5-3M	5		< DL
	WASH 2	HCl 2.5M	5		< DL
	ELUITION2	water	0.7	<DL*	2.184

The Sc recovery yield is considered to be quantitative since all the amount of Sc in the mock solution is completely recovered in the ELUTION sample.

The two DGA resins procedure (#6) (Figure 28) has turned to be the best separation/purification keeping Ti below the ICP-OES detection limit (<0.2ppm). This procedure lasts about 20 minutes and is easily automatable.

FIGURE 28. SCHEMA OF THE SC/TI SEPARATION USING DGA-EXTRACTION CHROMATOGRAPHIC RESIN (LEFT); PICTURE OF THE LOADING PHASE ON A DGA RESIN (RIGHT)

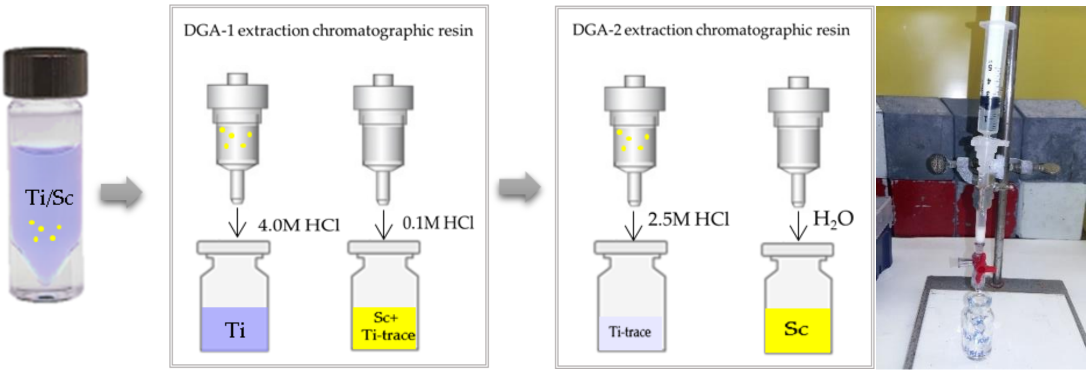

Domnanich, K.A.; Eichler, R.; Müller, C.; Jordi, S.; Yakusheva, V.; Braccini, S.; Behe, M.; Schibli, R.; Türler, A.; van der Meulen, N.P. Production and separation of ^{43}Sc for radiopharmaceutical purposes. *EJNMMI Radiopharmacy and Chemistry* 2017, 2:14, DOI: 10.1186/s41181-017-0033-9.

Pourmand, A.; Dauphas, N. Distribution coefficients of 60 elements on TODGA resin: application to ca, Lu, Hf, U and Th isotope geochemistry. Talanta 2010, *81*, 741–53, DOI:10.1016/j.talanta.2010.01.008

3. Congressi, pubblicazioni, tesi, seminari (2018)

- **Organizzazione al 2° incontro del CRP promosso da IAEA su "Therapeutic Radiopharmaceuticals labelled with new emerging radionuclides (^{67}Cu, ^{186}Re, ^{47}Sc)"**, Legnaro 5-9 March; presentazione orale, redazione documento finale, G. Pupillo
- **Relazione su invito alla conferenza 15th International Conference on Nuclear Reaction Mechanisms**, Varenna, June 11-15, 2018; section "Medical Radioisotopes", "Cyclotron-based production of the theranostic radionuclides ^{67}Cu and ^{47}Sc", G. Pupillo et al.
- **Presentazione orale presso 15th International Conference on Nuclear Reaction Mechanisms**, Varenna, June 11-15, 2018; section "Medical Radioisotopes", "Challenges in the modeling of nuclear reactions for theranostic applications", A. Fontana et al.
- **Presentazione orale presso 2018 European Nuclear Physics Conference**, Bologna, 2-7 Settembre, "Nuclear cross section measurements of the theranostic radionuclide Sc-47: Preliminary results of the PASTA project", G. Pupillo et al.
- **Presentazione poster presso 41st European Cyclotron Progress Meeting**, 2-6 September, Dubna, Russia, "High energy Vibrational Powder Plating for cyclotron target deposition" H. Skliarova et al.
- **Presentazione poster presso Terachem 2018**, September 26-29, Bressanone, "LARAMED: a LAboratory of RAdioisotopes for MEDicine" P. Martini et al.
- **Invito al Technical Meeting IAEA on "Nuclear Data for Medical Applications"**, Vienna 10-13 Dicembre, "Cross section measurements at the Arronax facility for the production of Cu-67 and Sc-47 and related nuclear data needs" G. Pupillo et al.

- **Invito al Technical Meeting IAEA on "Nuclear Data for Medical Applications"** , Vienna 10-13 Dicembre, "Model study of Sc-47 production at low/intermediate-energy cyclotrons and data needs" L. Canton et al.

Proceeding conferenze:

15th International Conference on Nuclear Reaction Mechanisms (in press):

- G. Pupillo et al., Cyclotron-based production of the theranostic radionuclides ^{67}Cu and ^{47}Sc
- A. Fontana et al., Challenges in the modelling of nuclear reactions for the theranostic applications

EuNPC-2018 (in press):

- G. Pupillo et al., Preliminary results of the PASTA project

LANSPA&WONP-NURT 2017 (in press):

- L. Canton et al., The modeling of reaction cross sections in the production of theranostic radionuclides

Tesi:

- **Simone Calzaferri**, Tesi di Laurea Magistrale A.A. 2017/2018, *Production of ^{47}Sc for Theragnostic Applications in Nuclear Medicine*, Università di Pavia, Relatore: A. Fontana, Correlatore: L. Canton

- Da Settembre 2018 **Lucia De Dominicis** (Università di Bologna) svolge la sua tesi specialistica in fisica (relatore interno: Prof. Mauro Bruno) su argomenti relativi il progetto PASTA, in particolare l'analisi dati degli irraggiamenti effettuati su bersagli di Vanadio naturale.

Seminari:

- Seminario presso LNL, 3 Luglio 2018 "Cross section measurements for the production of the theranostic radionuclides Cu-67 and Sc-47: Results from COME and PASTA projects", G. Pupillo

- Seminario divulgativo organizzato dall'associazione Scienza in un bicchiere, 22 Novembre 2018, Castelfranco Veneto, titolo "La fisica nucleare al servizio della medicina", G. Pupillo